

Thermal dilepton production within conformal viscous Gubser flow

Lakshmi J. Naik* and V. Sreekanth†

Department of Physics, Amrita School of Physical Sciences, Coimbatore, Amrita Vishwa Vidyapeetham, India

(Dated: June 3, 2025)

By employing the Gubser solutions of causal relativistic second-order Israel-Stewart hydrodynamics, we study the thermal dilepton production from heavy-ion collisions, considering the transverse expansion of the viscous hot QCD medium along with longitudinal boost-invariance. We analyze the evolution of the temperature and shear stress profiles of the QCD matter under Gubser flow for different values of the associated parameter q (inverse length scale). We study the dilepton production using leading order Born rates from QGP and hadronic sectors under Gubser geometry. Viscous modified dilepton rate is calculated using the first-order Chapman-Enskog (CE) like non-equilibrium correction of the particle distribution function. Our study indicates that lower values of q result in the enhancement of the emitted dilepton spectra. We also determine the effective temperature of the hot QCD medium from the inverse slope of transverse mass spectra, for different q . We find that the effective temperature determined from the dilepton spectra for a smaller system to be higher. Further, we compare the strength of CE like and Grad's viscous correction to the ideal dilepton spectra and find that CE type viscous corrections are well behaved compared to that of Grad's in the presence of transverse flow.

I. INTRODUCTION

The ultra-relativistic heavy-ion collision experiments provide an opportunity to explore various aspects of the strongly interacting hot and/or dense nuclear matter called Quark-Gluon Plasma (QGP). Analysis of the experimental data from these collisions imply that the QGP behaves like a near perfect fluid with extremely low value of shear viscosity to entropy density ratio, $\eta/s = 1/4\pi$ [1–9]. This has invoked interest in employing relativistic dissipative hydrodynamics to model the expansion of QGP fireball in heavy ion collisions [10, 11]. Hydrodynamics describes the QGP very close to thermal equilibrium and QCD kinetic theory calculations bring an insight on how the system attains this thermal equilibrium [12].

It has been now well accepted that the evolution of QGP can be described using relativistic viscous hydrodynamics [13–15]. The relativistic first-order Navier-Stokes theory [16, 17] exhibits acausal behaviour [18–20] and this has led to the development of causal higher order dissipative theories. Recently, several second-order relativistic dissipative hydrodynamic theories have been formulated and applied in the context of heavy-ion collisions [15]. Some of the relativistic second-order dissipative hydrodynamic formalisms derived can be found in following works [21–29]. Similarly, several formalisms of relativistic third-order theories based on different frameworks also exist [30–33]. Recently, there have been attempts to develop first-order causal viscous theories as well [34–37].

The relativistic hydrodynamic equations can be solved by considering the geometry of heavy-ion collisions [38, 39]. The expansion of QGP is initially along the collision axis (z -axis) and later, transverse expansion also starts to build up. The simplest model which describes the dynamics of heavy-ion collisions at early proper times is the one-dimensional Björken flow [40]. The Björken's solution possess boost in-

variance along the longitudinal direction (z -axis) and translational invariance in the transverse plane. Gubser flow is a two-dimensional model considering both the longitudinal and transverse expansion of QGP, developed in Refs. [41, 42]. This model provides semi-realistic solutions to the hydrodynamic equations by invoking the conformal equation of state ($\epsilon = 3P$). The Gubser solutions are symmetric under the $SO(3)_q \otimes S(1, 1) \otimes \mathbf{Z}_2$ group transformations.

Gubser's solution has been employed in the context of heavy-ion collisions to study various aspects of the matter produced. Solutions of relativistic ideal hydrodynamics and first-order Navier-Stokes equation within the Gubser flow have been found and analysed [41, 42]. In Ref. [43], solutions of second-order Israel-Stewart (IS) theory have been derived within the same model. Later, an exact solution of relativistic Boltzmann equation was studied in the relaxation time approximation for system evolving under Gubser symmetry and it was found that the second-order hydrodynamic theories provide an overall good agreement with this solution [44, 45]. Further, solutions of anisotropic hydrodynamic equations have also been explored considering the Gubser flow in several works [46–48]. Within the same model, the analytical solutions of dissipative spin hydrodynamics have also been looked at recently [49].

A completely analytical description of elliptic flow (v_2) in relativistic dissipative hydrodynamics within Gubser model was obtained in Ref. [50]. Effect of magnetic field on directed flow v_1 was also investigated within Gubser flow [51]. In Ref. [52], the flow harmonics have been calculated analytically within an anisotropically perturbed Gubser flow and later, in Ref. [53], they were derived at finite density. Gubser flow has been employed in the study of quarkonia suppression in small systems [54]. Recently, thermal photon production within Gubser flow was analysed in Ref. [55], where the effect of viscosity was not included. In the present work, we intend to study another important signal from heavy-ion collisions - thermal dileptons, by considering the viscous QGP expansion modelled using Gubser flow within causal second-order IS relativistic hydrodynamics.

Electromagnetic signals such as dileptons and photons are

* jn_lakshmi@cb.students.amrita.edu

† v.sreekanth@cb.amrita.edu

emitted from all the stages of heavy-ion collisions. Since they escape from the fireball easily, they remain an important probe for the analysis of the properties of high temperature matter created [56–63]. Photon and dilepton production from different stages of the QGP evolution is studied by identifying major contributory mechanisms [64–73]. They can emanate majorly from the initial hard scatterings, medium induced thermal radiation and final stage hadronic decays and have proved to be a great source in understanding the properties of matter created [56, 58, 61]. Recently, photons and dileptons are shown to be very useful to probe the early-time pre-equilibrium states of the fireball as well [74–79].

Dileptons, despite being produced less compared to the photons, are advantageous as they have invariant mass (M) and hence can be separated from various sources. The presence of invariant mass leaves their spectra unaffected by the Doppler shifts, unlike the case of photons [80]. Drell-Yan process in the early times produces dileptons having very large invariant mass [81]. Dileptons from the QGP phase are dominantly produced in the intermediate mass range $1.1 \leq M(\text{GeV}) \leq 2.9$, while those from the hadronic decays are created in the low mass range $M < 1.1 \text{ GeV}$ [56, 59, 61]. In the QGP phase, the most dominant contribution is known to come from the thermal dileptons produced via the $q\bar{q}$ -annihilation. Another major source for thermal dileptons comes from the pion annihilation in the hadronic phase. The presence of dissipation in the QGP medium affects the production of these particles. The impact of viscosity on thermal particle production has been investigated using causal relativistic hydrodynamics and found to show appreciable effects on the spectra [82–89].

In the present work, we study the thermal dilepton spectra in presence of shear viscosity from heavy-ion collisions using the solutions of second-order IS theory within Gubser model. The effect of viscosity on the dilepton production rate is incorporated through the Chapman-Enskog like non-equilibrium distribution function which is known to have a rapid convergence up to second order [90]. Further, we determine an effective temperature of the QGP medium from analysing the obtained dilepton yield.

The paper is structured as follows. In Section II, we review the Gubser model. Causal second-order dissipative hydrodynamics of Israel-Stewart within Gubser flow is presented in Section III. We evaluate the dilepton yield within Gubser flow in Section IV. Section V is devoted to the results and its discussion. We summarize our results in Section VI.

Notations and conventions: Throughout the manuscript, we follow the metric convention $g_{\mu\nu} = \text{diag}(+1, -1, -1, -1)$. We take $c = 1$ in our calculations.

II. GUBSER FLOW

Milne coordinates $x^\mu = (\tau, r, \phi, \eta_s)$ are the most natural choice to describe the heavy-ion collision scenario at ultra-

relativistic energies and are expressed as

$$\begin{aligned}\tau &= \sqrt{t^2 - z^2}, & \eta_s &= \tanh^{-1}(z/t), \\ r &= \sqrt{x^2 + y^2}, & \phi &= \tan^{-1}(y/x).\end{aligned}\quad (1)$$

Here, τ and η_s denote the proper time and space-time rapidity respectively, r is the radial distance from the fireball center and ϕ is the azimuthal angle in the transverse plane. The Björken flow model [40] offers a simplified, yet essential, one-dimensional representation of QGP dynamics and evolution. This model can be expressed in terms of the above coordinate system with the line element given by $ds^2 = d\tau^2 - dr^2 - r^2 d\phi^2 - \tau^2 d\eta_s^2$ and fluid four-velocity $u^\mu = (1, 0, 0, 0)$. The Björken's prescription is based on several assumptions such as boost invariance along η_s direction, translational invariance in the transverse plane and symmetry under reflections along the η_s direction. Steven Gubser made a generalization of Björken flow by replacing the translational invariance with the conformal symmetry $SO(3)$, while the invariance under boosts and reflections still maintained [41]. Under the Gubser model, the system has a finite transverse size and it undergoes expansion along both radial and longitudinal directions. However, such a description is applicable only for a system of conformal fluids.

Gubser flow on a de-Sitter background is obtained by Weyl rescaling of the metric measure in Milne coordinates, *i.e.*, $ds^2 \rightarrow d\hat{s}^2 \equiv ds^2/\tau^2$, which is followed by a coordinate transformation from (τ, r) to the *Gubser coordinates* (ρ, θ) :

$$\sinh \rho \equiv -\frac{1 - (q\tau)^2 + (qr)^2}{2q\tau}, \quad (2)$$

$$\tan \theta \equiv \frac{2qr}{1 + (q\tau)^2 - (qr)^2}. \quad (3)$$

Note that, here q describes an arbitrary energy scale which represent the transverse size of the system. Note that, in the following, all the variables depending on the Gubser coordinates are denoted by a hat. Now, the Weyl rescaled line element in the new coordinates $\hat{x}^\mu = (\rho, \theta, \phi, \eta_s)$ is given by

$$d\hat{s}^2 = d\rho^2 - (\cosh^2 \rho d\theta^2 + \cosh^2 \rho \sin^2 \theta d\phi^2 + d\eta_s^2).$$

In the de Sitter coordinates, Gubser flow appears to be static *i.e.*, $\hat{u}^\mu = (1, 0, 0, 0)$; whereas, the Weyl rescaling makes all the macroscopic quantities dimensionless by scaling with appropriate powers of rescaling parameter τ . Further, the rescaling renders the fluid homogeneous, with all the fields depending only on the coordinate ρ . Note that the scalar expansion rate of the medium can be obtained as $\hat{\Theta} \equiv \hat{D}_\mu \hat{u}^\mu = 2 \tanh \rho$. Below, we note the transformation relations followed by the hydrodynamic fields in our analysis:

$$T(\tau, r) = \frac{\hat{T}}{\tau}, \quad (4)$$

$$\pi_{\mu\nu}(\tau, r) = \hat{\pi}_{\alpha\beta} \frac{1}{\tau^2} \frac{\partial \hat{x}^\alpha}{\partial x^\mu} \frac{\partial \hat{x}^\beta}{\partial x^\nu}. \quad (5)$$

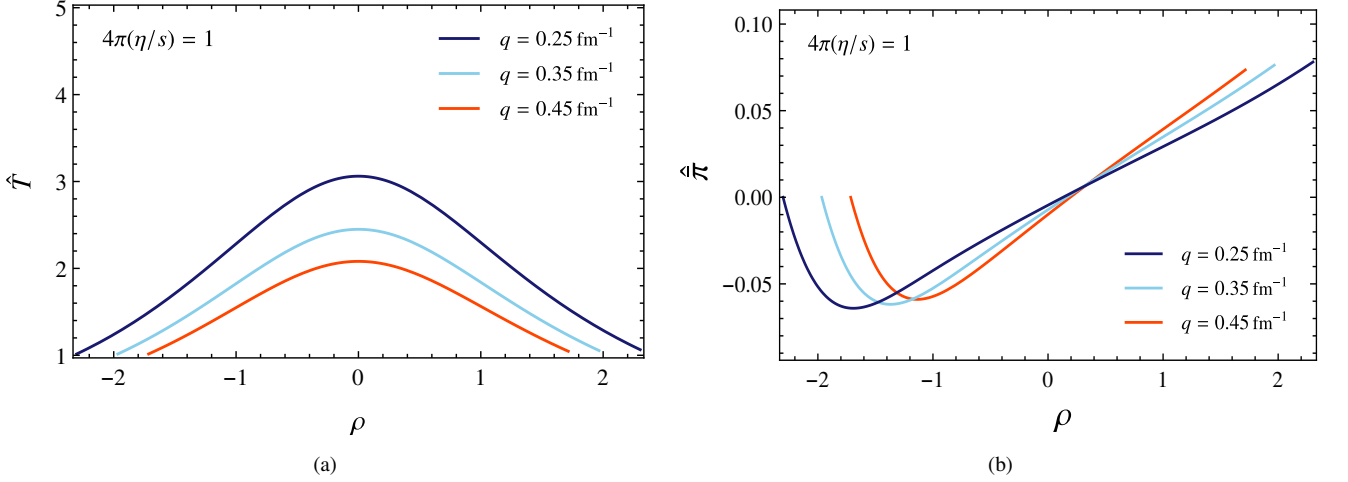


FIG. 1. (a) Temperature \hat{T} and (b) normalized shear stress profile $\hat{\pi} \equiv \hat{\pi}/(\hat{\epsilon} + \hat{P})$ of the hot QCD matter as a function of Gubser coordinate ρ for different values of q , with $4\pi(\eta/s) = 1$.

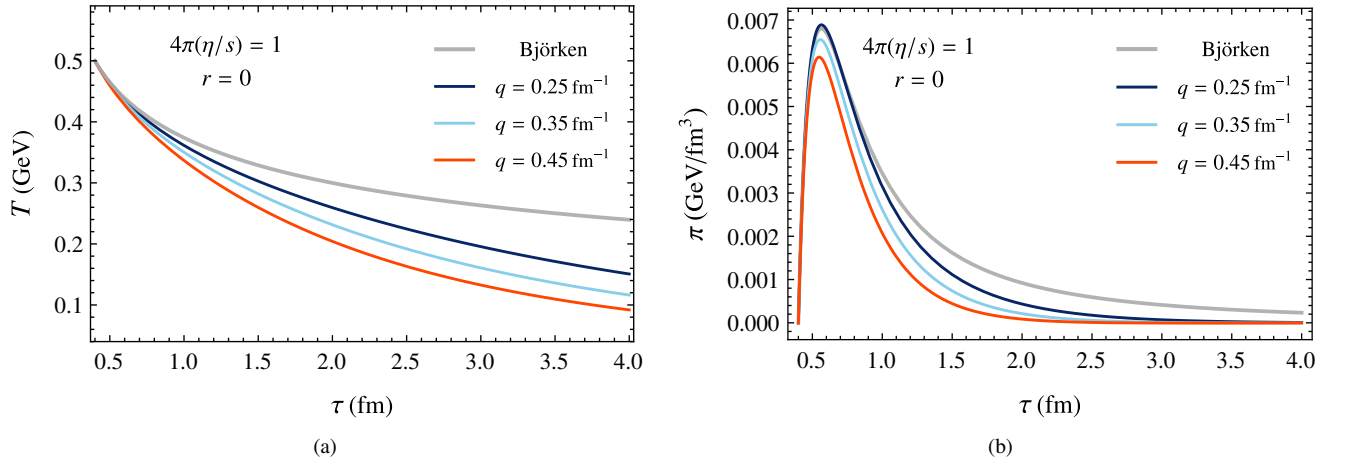


FIG. 2. (a) Temperature T and (b) shear stress π evolution of the hot QCD matter (at $r = 0$) as a function of Milne coordinate τ (proper time) for different values of q , with $4\pi(\eta/s) = 1$.

III. ISRAEL-STEWART THEORY WITHIN GUBSER FLOW

In this section, we briefly review the second-order Israel-Stewart hydrodynamics formulated within the Gubser model as derived in Ref. [43]. We begin by noting the energy-momentum tensor in Gubser coordinates for a viscous fluid with energy density $\hat{\epsilon}(\rho)$ and pressure $\hat{P}(\rho)$:

$$\hat{T}^{\mu\nu} = (\hat{\epsilon} + \hat{P})\hat{u}^\mu\hat{u}^\nu - \hat{P}\hat{g}^{\mu\nu} + \hat{\pi}^{\mu\nu}, \quad (6)$$

where $\hat{\pi}^{\mu\nu}(\rho)$ is the shear-stress tensor. Recall that, because of Weyl rescaling, all the hydrodynamic quantities are dimensionless with functional dependence only on the coordinate ρ . Within this model, $\hat{\pi}_\nu^\mu$ is diagonal and is parameterized as

$$\hat{\pi}_\nu^\mu = \text{diag}(0, \hat{\pi}/2, \hat{\pi}/2, -\hat{\pi}), \quad (7)$$

We note that the form of shear stress tensor appears identical to that defined within Bjorken model. Also, $\hat{\pi}_\rho^\alpha = 0$ (for

$\alpha = \rho, \theta, \phi, \eta_s$), which implies orthogonality to the flow profile. The evolution for $\hat{\epsilon}$ and $\hat{\pi}$ can be obtained by solving the nonlinear equations of motion [43]:

$$\frac{d\hat{\epsilon}}{d\rho} + \frac{8}{3}\hat{\epsilon}\tanh\rho - \hat{\pi}\tanh\rho = 0, \quad (8)$$

$$\hat{\tau}_\pi \frac{d\hat{\pi}}{d\rho} + \hat{\pi} + \frac{8}{3}\hat{\tau}_\pi\hat{\pi}\tanh\rho - \frac{16}{9}\frac{\eta}{s}\frac{\hat{\epsilon}}{\hat{T}}\tanh\rho = 0, \quad (9)$$

where $\hat{\tau}_\pi$ is the shear relaxation time, proportional to shear viscosity to entropy density ratio η/s . The above equations constitute the Israel-Stewart (IS) hydrodynamic theory within Gubser flow. These equations can be solved by employing an equation of state (EoS) to close the set. We use the relativistic conformal EoS for an ideal gas of massless quarks and gluons given by

$$\hat{\epsilon} = 3\hat{P} = 3 \left[2(N_c^2 - 1) + \frac{7}{2}N_c N_f \right] \frac{\pi^2}{90} \hat{T}^4, \quad (10)$$

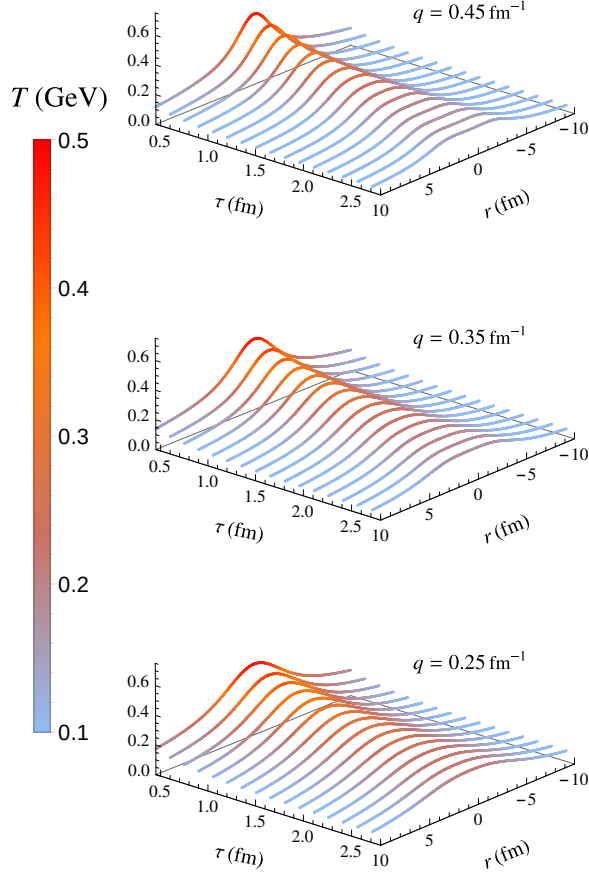


FIG. 3. Temperature of QGP obtained by solving the IS hydrodynamics within Gubser flow, for different values of q . We have taken the viscosity to be $4\pi(\eta/s) = 1$ for this analysis.

where $N_c = 3$ and $N_f = 2$ are the number of colors and flavors of quarks respectively. For a conformal fluid, $\eta \sim s$ and the relaxation time must be proportional to the inverse of temperature and we fix $\hat{\tau}_\pi = 5(\eta/s)/\hat{T}$ motivated by kinetic theory [25].

In the absence of viscosity, Eqs. (8) and (9) reduce to a single equation for temperature, and the analytical solution of the same is given by [41, 42]

$$\hat{T}_i(\rho) = \frac{\hat{T}(\rho_0)}{\cosh^{2/3} \rho}; \quad (11)$$

where $\hat{T}(\rho_0) = \tau_0 T(\tau_0, r = 0)$, $T(\tau_0, r = 0)$ is the initial temperature and τ_0 denote the initial proper time.

Now, we study the evolution of temperature and shear stress profiles of hot QCD matter obtained by numerically solving the above IS hydrodynamic equations of motion. We take the initial proper time for the hydrodynamical evolution of the system as $\tau_0 = 0.4$ fm, in line with QGP thermalization time estimates [91]. It is known that the hydrodynamic description of the system is valid when the universal scal-

ing time $\tilde{\omega} \equiv T\tau/(4\pi\eta/s) \approx 1$ [92]. We note that all the values of initial conditions used in this work confines within $\tilde{\omega} \approx 1$. We choose the relevant initial conditions [55]: $T_0 = T(\tau_0, r = 0) = 0.5$ GeV and $\pi_0 = \pi(\tau_0, r = 0) = 0$ with $\tau_0 = 0.4$ fm. In Gubser coordinates, these correspond to $\hat{T}(\rho_0) = 1.02$ and $\hat{\pi}(\rho_0) = 0$. The value of ρ_0 depends on the arbitrary length scale q considered, and we determine the same from Eq. (2). We have taken $4\pi(\eta/s) = 1$ and the parameter $q = 0.25, 0.35$ and 0.45 fm $^{-1}$ in our analysis, corresponding to the relevant transverse system size values. Later, we also vary viscosity as $4\pi(\eta/s) = 1$ and 2 in our studies. In order to compare with one-dimensional boost invariant evolution of the system, we solve the IS equations in Milne coordinates for Björken flow [93]

$$\frac{d\epsilon}{d\tau} + \frac{\epsilon + P - \pi}{\tau} = 0, \quad (12)$$

$$\tau_\pi \frac{d\pi}{d\tau} + \pi + \left(\frac{4}{3} + \lambda\right) \tau_\pi \frac{\pi}{\tau} - \frac{4}{3} \frac{\eta}{\tau} = 0, \quad (13)$$

where $\pi = \pi_{\eta_s}^{\eta_s}$, $\lambda = 10/21$ and $\tau_\pi = 5(\eta/s)/T$.

We plot the temperature \hat{T} and normalized shear stress $\hat{\pi} \equiv \hat{\pi}/(\hat{\epsilon} + \hat{P})$ profiles as a function of the Gubser coordinate ρ , obtained by solving Eqs. (8) and (9), for different q in Fig. 1, with $4\pi(\eta/s) = 1$. It is observed that the system moves away from the initial state: $\hat{T}(\rho_0) = 1.02$, $\hat{\pi}(\rho_0) = 0$ due to the initial rapid longitudinal expansion and as ρ increases, the system passes through the equilibrium state ($\hat{\pi} = 0$) again. From Fig. 1(a), we see that the temperature of the system has a maximum value at $\rho = 0$ and then decreases symmetrically with increment in $|\rho|$. With the increase in q , the maximum value of \hat{T} observed at $\rho = 0$ descends and the temperature profile flattens. Similarly, from Fig. 1(b), we find that the value of $\hat{\pi}$ first decreases below zero and reaches a minimum, then with the increase in ρ , $\hat{\pi}$ also increases and passes through the initial state at $\rho = 0$. For further increment in ρ , $\hat{\pi}$ keep on increasing. We observe that the minimum value of $\hat{\pi}$ occurs at less negative value of ρ , when q is increased.

Now, using the more familiar Milne coordinates (τ and r), we study the space-time dependence of temperature and shear-stress of hot QCD matter for different values of q . In subsequent analyses, we use fixed value of initial temperature and proper time $T_0 = 0.5$ GeV and $\tau_0 = 0.4$ fm. In Fig. 2, we plot the proper-time evolution of T and π at $r = 0$, with $4\pi(\eta/s) = 1$. We also plot the evolution corresponding to the Björken case for comparison. From Fig. 2(a), we observe that the temperature of the system takes longer time to cool for smaller values of q . This is because the scalar expansion rate within Gubser model, $\hat{\Theta} = 2 \tanh \rho$ depends on the parameter q and smaller values of q slow down the rate of expansion which result in slower cooling of the medium. Also, we note that the temperature profile approaches the Björken case as $q \rightarrow 0$. In Fig. 2(b), we show the proper-time evolution of π within Gubser model, at $r = 0$. We observe that the effect of shear viscous pressure is large at early times. The impact of shear stress increases with decrease in the value of q . For comparison, the shear stress evolution in Björken model is also shown. Note that the peak of π occurs almost at the same

τ for the Gubser and Björken cases since relaxation time is kept fixed throughout this analysis.

Next, we look into the complete T and π profiles by considering the transverse expansion. Fig. 3 shows the evolution of the system temperature in the presence of viscosity along the r and τ directions, by varying the parameter q . For any value of q , it is observed that the temperature profile has a peak around the center of the fireball *i.e.*, $r = 0$, at $\tau = \tau_0$; this peak flattens over the radial coordinate with increase in the proper time. We see that the width of the peak around $r = 0$ increases for smaller values of q ; which implies that more region near $r = 0$ remains at a higher temperature (region shown in red shade) for lower q value, and hence the system takes longer time to cool (indicated by blue shade).

Similarly, in Fig. 4, we depict the shear stress profile π as a function of r and τ , for different values of q . We note that the effect of shear pressure is more visible around the center of the system and at early proper times. At initial times, π profile begins from a positive peak value at $r = 0$ and approaches a negative peak with increment in r and then increases finally to zero for large r values. As τ increases, in the region near $r = 0$ (shown in red), π first increases and reaches a positive maximum value, then starts to decrease and finally approaches zero. Whereas, as we move away from the centre (*i.e.* region depicted in blue), as τ evolves, π monotonously increases from the negative values to zero. It can be seen that, with sufficient increment in τ , the negative peaks observed at either side of $r = 0$ decreases and flatten over r to the value $\pi = 0$. Further, when q is increased from 0.25 to 0.45 fm^{-1} , the width of initial π profile decreases. Also we observe that, for large q , the shear stress evolution happens faster.

IV. THERMAL DILEPTON SPECTRA WITHIN GUBSER FLOW

In this section, we obtain the thermal dilepton spectra from heavy-ion collisions by employing the Gubser symmetry. Dileptons are emitted from all the stages of collisions through various mechanisms and probe the entire temperature history of collisions. Here, we focus on the dominant mechanisms of thermal dilepton production from QGP and hadronic phases. The major contribution of thermal dilepton emission from QGP medium comes from the $q\bar{q}$ -annihilation process, $q\bar{q} \rightarrow \gamma^* \rightarrow l^+l^-$ and in the hadronic phase, $\pi^+\pi^-$ -annihilation, $\pi^+\pi^- \rightarrow \rho^0 \rightarrow l^+l^-$ contributes dominantly to the spectra. From relativistic kinetic theory, the rate of dilepton production for these processes is given by [94]

$$\frac{dN}{d^4x d^4p} = \int \frac{d^3\mathbf{p}_1}{(2\pi)^3} \frac{d^3\mathbf{p}_2}{(2\pi)^3} \frac{M^2 g^2 \sigma(M^2)}{2E_1 E_2} \times f_q(\mathbf{p}_1) f_q(\mathbf{p}_2) \delta^4(p - p_1 - p_2). \quad (14)$$

In the above expression, $p_{1,2} = (E_{1,2}, \mathbf{p}_{1,2})$ denote the four-momenta of incoming particles having masses $m_{1,2}$. Four-momentum of the lepton pair is $p = (E = E_1 + E_2, \mathbf{p} = \mathbf{p}_1 + \mathbf{p}_2)$. Here, $\sigma(M^2)$ represent the cross-section for the process in the Born approximation, where

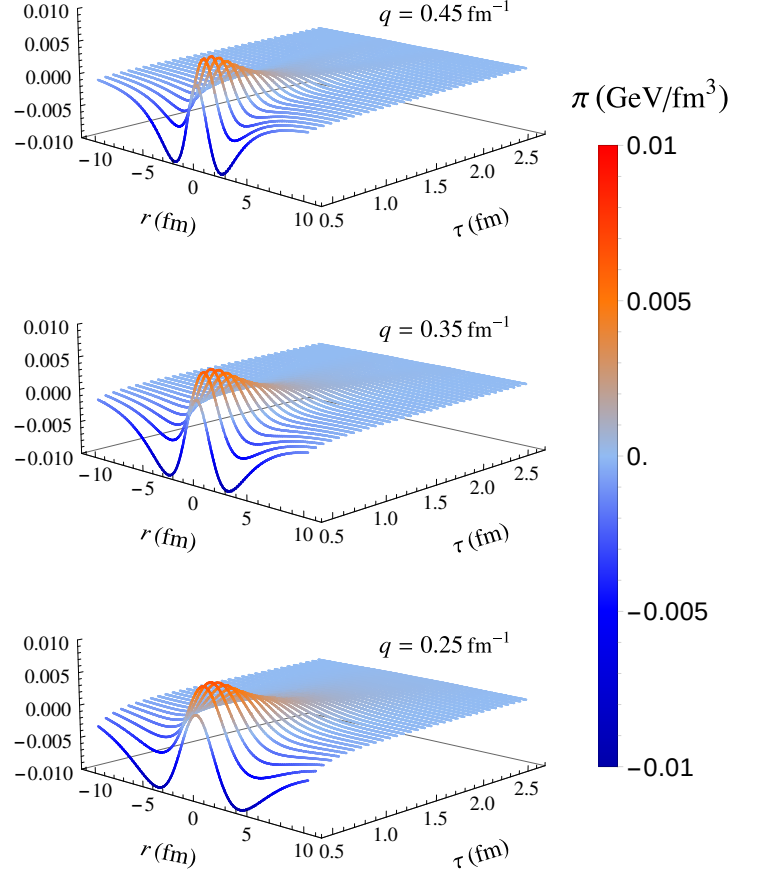


FIG. 4. Shear stress evolution of QGP obtained by solving the IS hydrodynamics within Gubser flow, for different values of q , with $4\pi(\eta/s) = 1$.

$M^2 = (E_1 + E_2)^2 - (\mathbf{p}_1 + \mathbf{p}_2)^2$ denotes the invariant mass of the virtual photon, and g is the degeneracy factor. Taking $N_f = 2$ and $N_c = 3$, we have $M^2 g^2 \sigma_q(M^2) = 80\pi/9\alpha_e^2$ for the $q\bar{q}$ -annihilation process in QGP phase, with α_e being the electromagnetic coupling constant. Also, we have $M^2 g^2 \sigma_\pi(M^2) = (4\pi/3)\alpha_e^2 |F_\pi(M^2)|^2$ [94] for $\pi^+\pi^-$ -annihilation in the hadronic phase. The term $|F_\pi(M^2)|^2 = m_\rho^4 / [(m_\rho^2 - M^2)^2 + m_\rho^2 \Gamma_\rho^2]$ is the electromagnetic pion form factor with $m_\rho = 775 \text{ MeV}$ and $\Gamma_\rho = 149 \text{ MeV}$ being the mass and decay width of $\rho(770)$ meson respectively [95]. Further, $f_i(\mathbf{p}_{1,2})$ are the phase-space distribution functions of interacting particles, where $i \equiv (q, \pi)$.

Presence of viscosity affects the dilepton production in two ways: first, through the hydrodynamic expansion of hot QCD medium and second through the distribution function. Viscous modifications to the phase-space distribution functions can be taken as $f_i = f_i^0 + \delta f_i$, where δf_i denotes the correction due to viscosity and f_i^0 is the equilibrium distribution function. Here, we use the δf_i upto first-order obtained from the Chapman-

Enskog like method [90]

$$\delta f_i = \frac{f_i^0 \beta}{2\beta_\pi (u \cdot p)} p^\mu p^\nu \pi_{\mu\nu}, \quad (15)$$

where $\beta = 1/T$ and $\beta_\pi = (\epsilon + P)/5$. By assuming the Maxwell-Boltzmann form for the equilibrium part and substituting the viscous modified distribution function in Eq. (14),

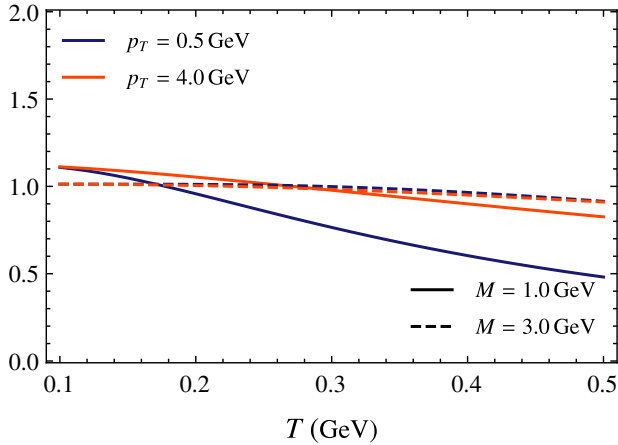
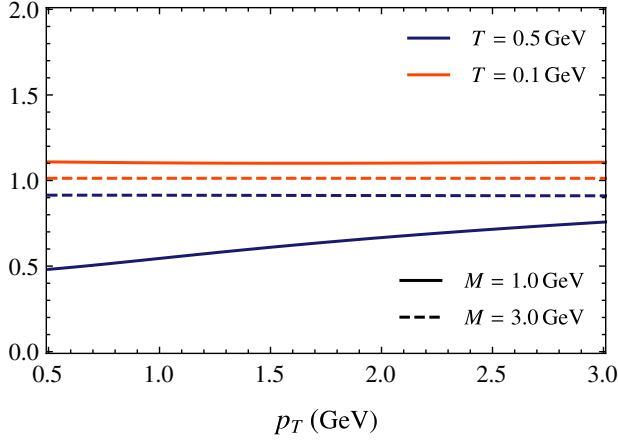
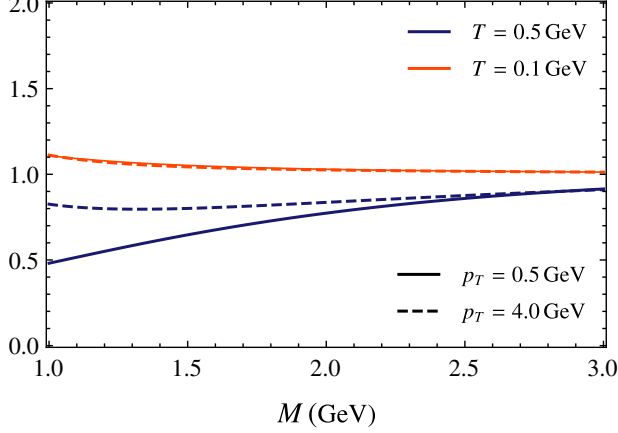


FIG. 5. Ratio of thermal dilepton rate from hadronic medium considering the massless pion approximation ($m_\pi = 0$) to that calculated with $m_\pi = 0.139$ GeV.

the expression for dilepton rate (keeping the terms upto second order in momenta) can be written as the sum of ideal and shear viscous contributions

$$\frac{dN}{d^4x d^4p} = \frac{dN^0}{d^4x d^4p} + \frac{dN^\pi}{d^4x d^4p}. \quad (16)$$

Now, the ideal contribution to the dilepton rate is obtained as [94]

$$\frac{dN^0}{d^4x d^4p} = \frac{1}{2} \sum_{i=q,\pi} \mathcal{R}_i e^{-u \cdot p/T}, \quad (17)$$

where $\mathcal{R}_i = M^2 g^2 \sigma_i(M^2)/(2\pi)^5$. We obtain the shear viscous part of dilepton rate as [96, 97]

$$\begin{aligned} \frac{dN^\pi}{d^4x d^4p} = & \frac{\beta}{\beta_\pi} \frac{p^\mu p^\nu \pi_{\mu\nu}}{2\mathcal{E}^5} \left(\mathcal{E} \left[\mathcal{E}^2 - \frac{3}{2} M^2 \right] (u \cdot p) \right. \\ & \left. + \frac{3}{4} M^4 \ln \left[\frac{(u \cdot p) + \mathcal{E}}{(u \cdot p) - \mathcal{E}} \right] \right) \frac{dN^0}{d^4x d^4p}; \end{aligned} \quad (18)$$

where, $\mathcal{E}^2 = (u \cdot p)^2 - M^2$.

The above rate expressions (Eqs. (17) and (18)) are integrated over the space-time history of heavy-ion collisions along with the temperature and shear stress tensor profiles of hot quark-gluon matter to obtain the thermal dilepton yield.

We now obtain the quantities $(u \cdot p)$ and $p^\mu p^\nu \pi_{\mu\nu}$ appearing in the dilepton rate expressions under Gubser flow. The four-momentum of the dileptons can be parameterized as $p^\mu = (m_T \cosh(y - \eta_s), p_T \cos(\phi_p - \phi), p_T \sin(\phi_p - \phi)/r, m_T \sinh(y - \eta_s)/\tau)$; where $m_T = \sqrt{p_T^2 + M^2}$ is the transverse mass of the dilepton, with p_T and M are its transverse momentum and invariant mass respectively. Also, ϕ_p is the phase angle and y denotes the rapidity of the particle. Using the definitions of \hat{u}^μ and $\hat{\pi}^{\mu\nu}$ within Gubser flow, along with p^μ , we obtain the factors appearing in the rate expressions as:

$$\begin{aligned} u \cdot p &= u_\tau m_T \cosh(y - \eta_s) - u_r p_T \cos(\phi_p - \phi), \quad (19) \\ p^\mu p^\nu \pi_{\mu\nu} &= m_T^2 \left(\cosh^2(y - \eta_s) \pi_{\tau\tau} + \frac{\sinh^2(y - \eta_s)}{\tau^2} \pi_{\eta_s \eta_s} \right) \\ &+ p_T^2 \left(\cos^2(\phi_p - \phi) \pi_{rr} + \frac{\sin^2(\phi_p - \phi)}{r^2} \pi_{\phi\phi} \right); \end{aligned} \quad (20)$$

where

$$u_\tau = \frac{\partial \rho}{\partial \tau} u_\rho = \frac{1}{\sqrt{1 - v_r(\tau, r)^2}}, \quad (21)$$

$$u_r = \frac{\partial \rho}{\partial r} u_\rho = \frac{-v_r(\tau, r)}{\sqrt{1 - v_r(\tau, r)^2}}; \quad (22)$$

with

$$v_r(\tau, r) = \frac{2q^2 \tau r}{1 + (q\tau)^2 + (qr)^2};$$

and

$$\pi_{\tau\tau} = -\frac{\hat{\pi}}{2\tau^2} \left(\frac{\partial\theta}{\partial\tau} \right)^2 \cosh^2 \rho, \quad (23)$$

$$\pi_{rr} = -\frac{\hat{\pi}}{2\tau^2} \left(\frac{\partial\theta}{\partial r} \right)^2 \cosh^2 \rho, \quad (24)$$

$$\pi_{\phi\phi} = -\frac{\hat{\pi}}{2\tau^2} \cosh^2 \rho \sin^2 \theta; \quad (25)$$

with

$$\pi_{\eta_s\eta_s} = \frac{\hat{\pi}}{\tau^2}. \quad (26)$$

Noting the four-dimensional volume element to be $d^4x = \tau d\tau r dr d\phi d\eta_s$, the dilepton yield from heavy-ion collisions within the Gubser flow can be now calculated as

$$\begin{aligned} \frac{dN}{dM p_T dp_T dy} &= M \int_0^{2\pi} d\phi_p \int_{\tau_0}^{\infty} \tau d\tau \int_0^{\infty} r dr \int_0^{2\pi} d\phi \\ &\times \int_{-\infty}^{\infty} d\eta_s \left[\frac{dN}{d^4x d^4p} \right] \Theta(T > T_{\min}), \end{aligned} \quad (27)$$

where the Heaviside step function (Θ) restricts the evolution of temperature till T_{\min} . The ideal contribution to the thermal dilepton yield can be simplified by performing the integrals over η_s and ϕ analytically using the integral representation of modified Bessel functions of first ($K_n(z)$) and second ($I_n(z)$) kinds respectively given in Appendix. A. The expression for ideal part of the dilepton yield can be now written as

$$\begin{aligned} \frac{dN^0}{dM p_T dp_T dy} &= 2\pi M \sum_{i=q,\pi} \mathcal{R}_i \int_0^{2\pi} d\phi_p \int_{\tau_0}^{\tau_f} \tau d\tau \int_0^{\infty} r dr \\ &\times K_0 \left[\frac{u_\tau m_T}{T} \right] I_0 \left[\frac{-u_r p_T}{T} \right] \Theta(T > T_{\min}). \end{aligned} \quad (28)$$

Similarly, the p_T integrated differential yield $dN/dM dy$ is obtained as

$$\frac{dN}{dM dy} = \int_{p_T^{\min}}^{p_T^{\max}} p_T dp_T \left[\frac{dN}{dM p_T dp_T dy} \right]. \quad (29)$$

By employing the temperature and viscous (π) profiles of the hot fireball obtained in the previous section, we numerically evaluate Eqs. (27) and (29) to obtain the dilepton spectra.

Further, for comparison with Chapman-Enskog like distribution function, we calculate the dilepton yield using the 14-moment Grad's non-equilibrium correction [98]

$$\delta f_G = \frac{f^0}{2sT^3} p^\mu p^\nu \pi_{\mu\nu}. \quad (30)$$

The shear viscous contribution to the dilepton rate due to the above correction is obtained as [82]

$$\frac{dN_G^\pi}{d^4x d^4p} = \frac{2}{3} \left(\frac{p^\mu p^\nu}{2sT^3} \pi_{\mu\nu} \right) \frac{dN^0}{d^4x d^4p}, \quad (31)$$

where $s = (\epsilon + P)/T$ is the entropy density. The ideal part is given by Eq. (17). One can obtain the corresponding dilepton yield within Gubser geometry in similar manner by making use of the expressions discussed before.

Before we proceed towards numerical evaluation of the dilepton yields within Gubser flow in the next session, we would like to comment on the validity of the assumption $m_\pi = 0$ in the dilepton rate calculation from hadronic medium. We plot the ratio of dilepton rate (ideal case) from hadronic phase calculated by considering the massless pion approximation to that obtained with non-zero mass $m_\pi = 0.139$ GeV, by varying M , p_T and T (keeping $p_z = 0$) in Fig. 5. While calculating the rate in the massive case, we have also used the Bose-Einstein distribution function for pions (See Appendix B for the rate calculation). We see that the approximation works better for all high values of M regardless of the p_T and T values considered (error remains less than 10%). At lower values of M , low p_T and high T result in more error. One can see that errors are well within 10%, except for the lower values of M and p_T ($\sim 50\%$ error). Therefore considering $m_\pi = 0$ is a reasonable approximation in our calculations and since Gubser flow is valid only with the conformal EoS, it is only consistent to use massless limit for pions in our study.

V. RESULTS AND DISCUSSION

In this section, we analyze the thermal dilepton spectra from heavy-ion collisions obtained by employing the solutions of Israel-Stewart hydrodynamics within Gubser flow. As already specified in Sec. III, we adopt the initial conditions $T(\tau_0, r = 0) = 0.5$ GeV, $\pi(\tau_0, r = 0) = 0$ at $\tau_0 = 0.4$ fm and we choose three different values of arbitrary energy scale, $q = 0.25, 0.35$, and 0.45 fm $^{-1}$ in our analysis. We make use of the temperature and shear stress profiles obtained in Sec. III by numerically solving Eqs. (8) and (9). Since we consider dileptons from both QGP and hadronic sources, we evolve the temperature up to a minimum value, $T(\tau_f, r) = T_{\min}$, where τ_f is the final proper time. Note that, here the value of τ_f depends on the coordinate r and hence matter at different radial distances from the center of fireball cool to T_{\min} at different proper times. The Heaviside Theta function $\Theta(T > T_{\min})$ in the dilepton yield expression takes this into consideration in our numerical analysis. Following Ref. [55], we take $T_{\min} = 0.1$ GeV. Also note that the yields are plotted for midrapidity region of dileptons *i.e.*, $y = 0$.

We first study the effect of variation of parameter q on the dilepton spectra by plotting the ideal dilepton yield in Fig. 6(a), for the invariant mass $M = 1.0$ GeV. The yield obtained within the Björken model, for the ideal temperature profile, $T(\tau) = T_0(\tau_0/\tau)^{1/3}$ is also shown for comparison. It is observed that there is an overall suppression in the spectra obtained for the Gubser flow for any q , compared to the Björken scenario. This is because, within the one-dimensional Björken model, temperature of QGP takes longer time to cool, in contrast to the Gubser case; as a result, the number of dileptons produced will be more. Also, it is seen that there is an

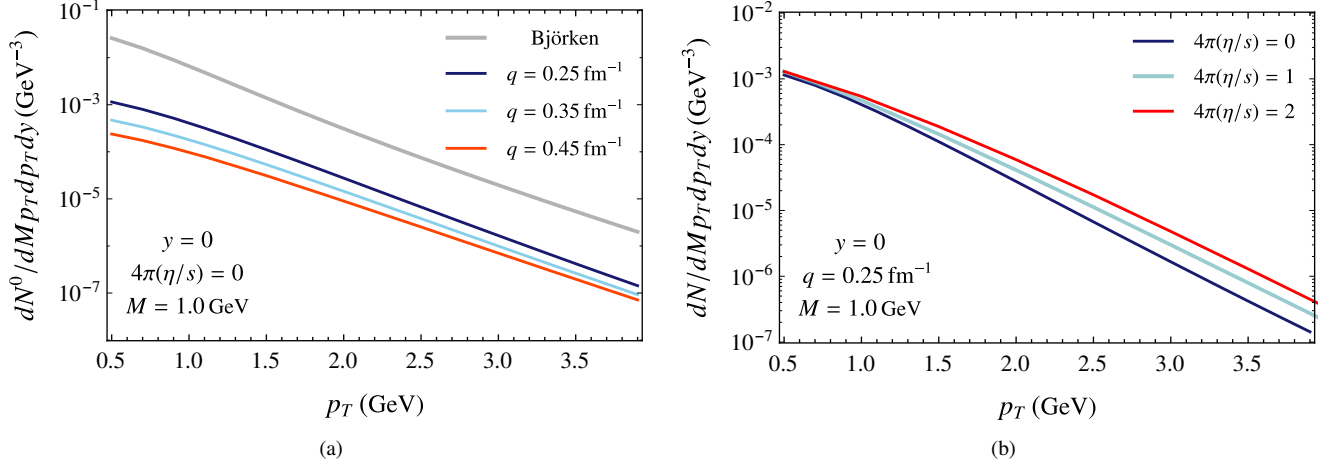


FIG. 6. (a) Thermal dilepton yield for relativistic ideal hydrodynamics by varying the arbitrary parameter q , with $M = 1.0$ GeV. The yield corresponding to the ideal Björken scenario ($q \rightarrow 0$) is also shown for comparison. (b) Thermal dilepton yield from IS hydrodynamics within Gubser flow by varying the viscosity, for $q = 0.25 \text{ fm}^{-1}$.

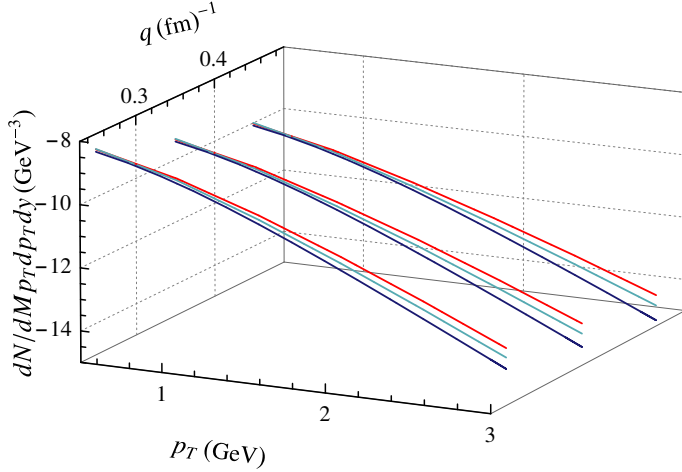


FIG. 7. Thermal dilepton yield from QGP and hadronic matter by varying the parameter q , for $M = 1.5$ GeV. The solid dark blue, light blue and red curves denote the yields corresponding to $4\pi(\eta/s) = 0, 1$ and 2 respectively.

overall decrement in the spectra with an increment in q value. This decrement is profound in the low p_T regime of the spectra. We note that, the parameter q is inversely related to the transverse radius/size of the fireball, $L = 1/q$. Therefore, an increment in q implies a decrease in the transverse size resulting in less production of lepton pairs. Further, we found that the spectra tend to approach the Björken case when $q \rightarrow 0$, as expected.

In order to understand whether the dilepton spectra from Gubser will approach to that of Björken, we vary M and p_T to high values and check their convergence. We keep the initial time ($\tau_0 = 0.4 \text{ fm}$) and temperature ($T_0 = 0.5 \text{ GeV}$) along with the final evolution temperature same for both the cases,

with $q = 0.45 \text{ fm}^{-1}$. We note that for the ideal Björken case, it takes $\sim 50 \text{ fm}$ to reach the $T_f = 0.1 \text{ GeV}$, whereas for the Gubser it is only $\sim 3.7 \text{ fm}$ at the center of the fireball ($r = 0$). It was found that even with very high values of M ($\sim 4 \text{ GeV}$) and p_T ($\sim 10 \text{ GeV}$), the Gubser spectra will not converge to that of Björken. Our studies indicate that the convergence of dilepton spectra within Gubser and Björken models happens only with the condition $q \rightarrow 0$.

Next, we analyze the effect of viscosity on the dilepton yield obtained within Gubser solutions of IS hydrodynamics in Fig. 6(b), by varying the viscosity. We fix the q value to be 0.25 fm^{-1} for this analysis. The solid dark blue curve denotes the ideal dilepton yield. We consider the viscosities $4\pi(\eta/s) = 1, 2$ and are represented using solid light blue, red curves respectively. The presence of viscosity enhances the dilepton yield, since incorporating the viscous corrections to the dilepton production rates result in positive contribution to the spectra. Also, the viscous effects in the medium slows down the expansion of the fireball and thereby increases the yield [84, 85]. In Fig. 7, we show the effect of variation of the parameter q on the viscous dilepton spectra for $M = 1.5 \text{ GeV}$ in a three-dimensional plot. As mentioned before, we observe an overall decrement in the dilepton spectra when q is increased.

In Fig. 8(a), we plot the p_T -integrated dilepton yield from both viscous and ideal hot QCD medium as a function of dilepton invariant mass M . For this analysis, we have fixed $q = 0.35 \text{ fm}^{-1}$ and for the viscous case, the viscosity is taken to be $4\pi(\eta/s) = 2$. The integration over p_T is carried out in the range: $1 \leq p_T \text{ (GeV)} \leq 20$ [99]. As expected, we find an overall enhancement in the invariant mass spectra due to the presence of viscosity and this increment is more profound for higher invariant masses. We note that the peak observed at $M = 0.77 \text{ GeV}$ is because of the dilepton production from $\rho(770)$ decay.

Next, in order to have a complete analysis of the thermal dileptons within viscous Gubser flow, we determine the effec-

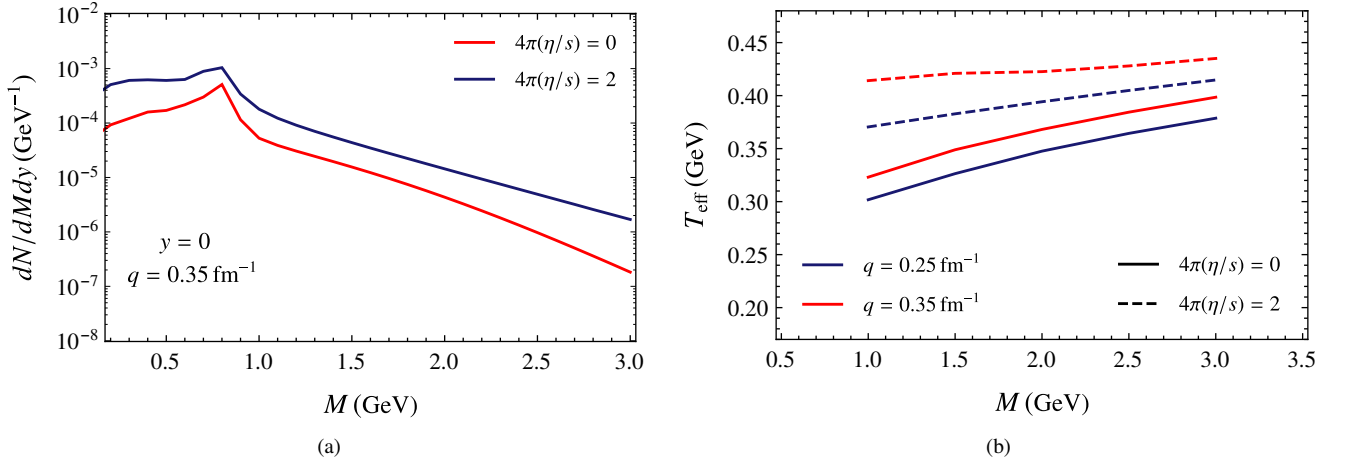


FIG. 8. (a) Dilepton invariant mass spectra from both viscous and inviscid expanding hot QCD medium, by fixing $q = 0.35 \text{ fm}^{-1}$. (b) Effective temperature of the system as a function of invariant mass of dilepton. Solid lines denote the ideal T_{eff} calculated from ideal spectra.

tive slope parameters of transverse momentum spectra. We follow the method outlined in Ref. [82] and calculate the effective temperature T_{eff} from the dilepton spectra as a function of invariant mass. We find T_{eff} by fitting the spectra at a fixed M with the expression:

$$\frac{dN}{dM^2 m_T dm_T dy} \propto \exp(-m_T/T_{\text{eff}}). \quad (32)$$

We choose the range $1.1 \leq p_T(\text{GeV}) \leq 2.1$ for this fit. In Fig. 8(b), we plot the T_{eff} determined for ideal and viscous dilepton spectra as a function of M , for different q values. There is an enhancement in the T_{eff} curve with increase in M , implying that the viscous corrections increase with M . We observe that the T_{eff} determined from transverse momentum spectra within viscous Gubser hydrodynamics is larger compared to that evaluated within ideal Gubser solution. Further, the T_{eff} values are high for large value of q , since the effective temperature is determined from the inverse slope of the spectra.

We must note that in the analysis so far, we have fixed the initial temperature $T(\tau_0, r=0) \equiv T_0$ while studying the variation of the q parameter. This results in different initial energy density profiles for the system with peak value at $r=0$ remaining the same but with narrowed radial spread, as we increase the q value (smaller system size). This corresponds to higher initial energy density for smaller systems, even though its total energy is lesser compared to larger systems. And as we saw, thermal spectra with such initial conditions give rise to higher effective temperature for a smaller system. We now fix the initial total energy (E_{tot}) of the system and vary q in the analysis, thus covering both the initial energy and system size effects. We first obtain the value of E_{tot} for $T_0 = 0.5 \text{ GeV}$ and $q = 0.25 \text{ fm}^{-1}$. Then fixing thus obtained E_{tot} value, we determine T_0 corresponding to $q = 0.35 \text{ fm}^{-1}$. This results in higher temperature or initial energy density value at $r=0$ for larger q , i.e., smaller system. Also, the initial energy density profile gets narrowed for large q , since E_{tot} is kept constant. In this scenario too, we find that smaller sys-

tem results in a higher effective temperature. While fixing T_0 , the temperature profile becomes increasingly localized around the center with increment in q . This leads to a larger fraction of the total emission of dileptons originating from hotter regions. In the second case, maintaining the same total energy in a smaller volume necessitates a higher initial temperature, again enhancing the emission of high-momentum particles. Although this trend may appear counter-intuitive when compared to phenomenological expectations that associate larger systems with higher temperatures, it arises naturally from the spatial structure of the energy density in conformal Gubser hydrodynamics. These observations highlight the fact that effective temperatures extracted from thermal spectra are sensitive not only to the magnitude of the initial temperature or energy, but also to their spatial distribution.

Finally, in Fig. 9, we compare the dilepton spectra obtained for Chapman-Enskog like viscous correction (Eq. (15)) with that obtained using 14-moment Grad's method (Eq. (30)), for various q values. We fix $M = 1.0 \text{ GeV}$ and $4\pi(\eta/s) = 1$ for this comparison with fixing the central temperature $T(\tau_0, r=0) = 0.5 \text{ GeV}$, as before. We plot the ratio defined by

$$R_{p_T} = \left[\frac{dN}{dM p_T dp_T dy} \right] / \left[\frac{dN^0}{dM p_T dp_T dy} \right], \quad (33)$$

which gives the non-equilibrium corrections to the ideal dilepton yield (Eq. (28)). It can be seen that the viscous corrections grow with p_T for any value of q . This can be understood from the term $p^\mu p^\nu \pi_{\mu\nu}$ (Eq. (20)) in the δf , which is proportional to p_T^2 . It must be noted that the Grad's viscous correction is larger compared to the CE-like correction for any value of p_T and q . This will result in higher particle spectra while employing δf_G [90]. Also, the difference between both the viscous corrections is found to increase for larger p_T values. Further, we see that the strength of viscous corrections increase with increment in the value of q . We conclude from this analysis that the CE like δf is more suitable to study particle production from heavy-ion collisions, as indicated by the earlier study using 1-D Björken flow [90].

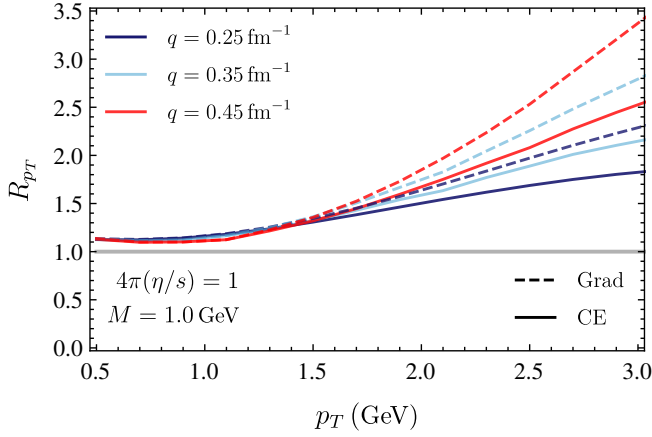


FIG. 9. Ratios of particle yields for Chapman-Enskog like (Eq. (15)) and Grad's (Eq. (30)) distribution functions for different q values.

VI. CONCLUSION

We have employed the solutions of second-order Israel-Stewart hydrodynamics within Gubser flow to investigate the thermal dilepton production from heavy-ion collisions. We calculated the dilepton rate in the presence of first-order Chapman-Enskog (CE) like viscous correction. The dilepton yield is calculated within Gubser model, which considers the transverse dynamics along with the longitudinal boost-invariance. The inclusion of radial dependence in the dilepton yield resulted in an overall decrement of the dilepton spectra compared to that obtained within 1-D Björken expansion. The radial expansion of QGP has profound impact on dilepton yields and we found that the dilepton spectra changes appreciably with variation in the value of arbitrary parameter q . We have also explored the effect of viscosity on the dilepton yields.

Further, we determined the effective temperature of QGP medium (T_{eff}) from the inverse slope of the transverse mass spectra obtained within Gubser flow. Our study reveals that in Gubser flow, smaller systems (larger q) yield higher effective temperatures, regardless of whether the initial condition fixes the temperature $T(\tau_0, r = 0)$ or total energy. This emanates from the increasingly localized energy density profiles in smaller systems, which enhance emission of particles from hotter regions. Our results emphasize that spatial geometry plays a critical role in shaping thermal spectra and effective temperature observables.

Finally, we have compared the strength of Chapman-Enskog (CE) like viscous correction to that of 14-moment Grad's and found that the strength of Grad's correction to the ideal dilepton yield is significantly high, especially at high p_T . Therefore, the CE like viscous correction is preferred over Grad's correction for studying the particle spectra. Furthermore, it will be interesting to employ the Gubser model to study the electromagnetic signals by considering CE like viscous corrections up to second-order. We leave this analysis for future study.

ACKNOWLEDGMENTS

Authors would like to thank the anonymous referee, whose suggestions have improved the quality of the manuscript. L. J. N. acknowledges the Department of Science and Technology, Government of India for the INSPIRE Fellowship.

Appendix A: Integral representation of modified Bessel functions

The expression for ideal contribution to dilepton yield Eq. (28) is obtained by using the following integral representations of modified Bessel functions of first and second kind respectively:

$$I_n(z) = \frac{1}{\sqrt{\pi}\Gamma(n+1/2)} (z/2)^n \int_0^\pi e^{-z \cos(t)} \sin^{2n}(t) dt,$$

$$K_n(z) = \frac{\sqrt{\pi}}{\Gamma(n+1/2)} (z/2)^n \int_0^\infty e^{-z \cosh(t)} \sinh^{2n}(t) dt,$$
(A1)

where $\Gamma(n)$ denotes the Gamma function.

Appendix B: Thermal dilepton production rate in hadronic medium considering massive pions

Here we derive the expression for thermal dilepton production rate in the hadronic medium by considering masses of incoming pions (m_π). We start with the expression

$$\frac{dN}{d^4x d^4p} = \int \frac{d^3\mathbf{p}_1}{(2\pi)^3} \frac{d^3\mathbf{p}_2}{(2\pi)^3} v_{\text{rel}} \sigma_\pi(M^2) \times f(\mathbf{p}_1) f(\mathbf{p}_2) \delta^4(p - p_1 - p_2),$$
(B1)

where $v_{\text{rel}} = \sqrt{M^2(M^2 - 4m_\pi^2)}/(2E_1 E_2)$ is the relative velocity and the cross-section is given by

$$\sigma_\pi(M^2) = \frac{4\pi\alpha^2}{3} \frac{|F_\pi(M^2)|^2}{M^2} \sqrt{1 - \frac{4m_\pi^2}{M^2}}.$$
(B2)

$f(\mathbf{p})$ is the Bose-Einstein distribution function. Integrating Eq. (B1) over \mathbf{p}_2 and expressing the momenta \mathbf{p} and \mathbf{p}_1 in terms of spherical polar coordinates, we obtain

$$\frac{dN}{d^4x d^4p} = \int_{p_{1\text{min}}}^{p_{1\text{max}}} \frac{d|\mathbf{p}_1|}{(2\pi)^5} |\mathbf{p}_1| \int_{-1}^{+1} d(\cos \theta) \times \frac{\sqrt{M^2(M^2 - 4m_\pi^2)}}{2E_1 |\mathbf{p}|} \sigma_\pi(M^2) \times f(\mathbf{p}_1) f(\mathbf{p} - \mathbf{p}_1) \delta(\cos \theta - \cos \theta_0),$$
(B3)

where $\cos \theta_0 = (2E \sqrt{|\mathbf{p}_1|^2 + m_\pi^2} - M^2)/2pp_1$. Now, performing the integral over the δ function, we get

$$\frac{dN}{d^4x d^4p} = \int_{p_{1\text{min}}}^{p_{1\text{max}}} \frac{d|\mathbf{p}_1|}{(2\pi)^5} |\mathbf{p}_1| \frac{\sqrt{M^2(M^2 - 4m_\pi^2)}}{2E_1 |\mathbf{p}|} \sigma_\pi(M^2) \times f(\mathbf{p}_1) f(\mathbf{p} - \mathbf{p}_1) \Big|_{\cos \theta_0}.$$
(B4)

The remaining $|\mathbf{p}_1|$ integral is evaluated numerically to obtain the dilepton rate with limits of integration fixed from $-1 \leq \cos \theta_0 \leq +1$. We use the above rate expression to compare with that obtained in the massless pion approximation in

Sec. IV. Note that in the limit $m_\pi = 0$ and while considering the Maxwell-Boltzmann statistics, Equation. (B4) reduces to the rate for pion annihilation in Eq. (17).

-
- [1] John Adams *et al.* (STAR), “Experimental and theoretical challenges in the search for the quark gluon plasma: The STAR Collaboration’s critical assessment of the evidence from RHIC collisions,” *Nucl. Phys. A* **757**, 102–183 (2005), [arXiv:nucl-ex/0501009](#).
 - [2] K. Adcox *et al.* (PHENIX), “Formation of dense partonic matter in relativistic nucleus-nucleus collisions at RHIC: Experimental evaluation by the PHENIX collaboration,” *Nucl. Phys. A* **757**, 184–283 (2005), [arXiv:nucl-ex/0410003](#).
 - [3] I. Arsene *et al.* (BRAHMS), “Quark gluon plasma and color glass condensate at RHIC? The Perspective from the BRAHMS experiment,” *Nucl. Phys. A* **757**, 1–27 (2005), [arXiv:nucl-ex/0405231](#).
 - [4] B. B. Back *et al.* (PHOBOS), “The PHOBOS perspective on discoveries at RHIC,” *Nucl. Phys. A* **757**, 28–101 (2005), [arXiv:nucl-ex/0410022](#).
 - [5] P. Kovtun, Dan T. Son, and Andrei O. Starinets, “Viscosity in strongly interacting quantum field theories from black hole physics,” *Phys. Rev. Lett.* **94**, 111601 (2005), [arXiv:hep-th/0405231](#).
 - [6] Tetsufumi Hirano and Miklos Gyulassy, “Perfect fluidity of the quark gluon plasma core as seen through its dissipative hadronic corona,” *Nucl. Phys. A* **769**, 71–94 (2006), [arXiv:nucl-th/0506049](#).
 - [7] Paul Romatschke and Ulrike Romatschke, “Viscosity Information from Relativistic Nuclear Collisions: How Perfect is the Fluid Observed at RHIC?” *Phys. Rev. Lett.* **99**, 172301 (2007), [arXiv:0706.1522 \[nucl-th\]](#).
 - [8] K. Aamodt *et al.* (ALICE), “Elliptic flow of charged particles in Pb-Pb collisions at 2.76 TeV,” *Phys. Rev. Lett.* **105**, 252302 (2010), [arXiv:1011.3914 \[nucl-ex\]](#).
 - [9] Ulrich Heinz and Raimond Snellings, “Collective flow and viscosity in relativistic heavy-ion collisions,” *Ann. Rev. Nucl. Part. Sci.* **63**, 123–151 (2013), [arXiv:1301.2826 \[nucl-th\]](#).
 - [10] Wit Busza, Krishna Rajagopal, and Wilke van der Schee, “Heavy Ion Collisions: The Big Picture, and the Big Questions,” *Ann. Rev. Nucl. Part. Sci.* **68**, 339–376 (2018), [arXiv:1802.04801 \[hep-ph\]](#).
 - [11] Paul Romatschke and Ulrike Romatschke, *Relativistic Fluid Dynamics In and Out of Equilibrium*, Cambridge Monographs on Mathematical Physics (Cambridge University Press, 2019) [arXiv:1712.05815 \[nucl-th\]](#).
 - [12] Jürgen Berges, Michal P. Heller, Aleksas Mazeliauskas, and Raju Venugopalan, “QCD thermalization: Ab initio approaches and interdisciplinary connections,” *Rev. Mod. Phys.* **93**, 035003 (2021), [arXiv:2005.12299 \[hep-th\]](#).
 - [13] Matthew Luzum and Paul Romatschke, “Conformal Relativistic Viscous Hydrodynamics: Applications to RHIC results at $s(\text{NN})^{1/2} = 200\text{-GeV}$,” *Phys. Rev. C* **78**, 034915 (2008), [Erratum: *Phys.Rev.C* **79**, 039903 (2009)], [arXiv:0804.4015 \[nucl-th\]](#).
 - [14] Amaresh Jaiswal and Victor Roy, “Relativistic hydrodynamics in heavy-ion collisions: general aspects and recent developments,” *Adv. High Energy Phys.* **2016**, 9623034 (2016), [arXiv:1605.08694 \[nucl-th\]](#).
 - [15] Gabriel S. Rocha, David Wagner, Gabriel S. Denicol, Jorge Noronha, and Dirk H. Rischke, “Theories of Relativistic Dissipative Fluid Dynamics,” *Entropy* **26**, 189 (2024), [arXiv:2311.15063 \[nucl-th\]](#).
 - [16] L. D. Landau and E. M. Lifshitz, *Fluid Mechanics* (1987).
 - [17] Carl Eckart, “The Thermodynamics of irreversible processes. 3.. Relativistic theory of the simple fluid,” *Phys. Rev.* **58**, 919–924 (1940).
 - [18] W. A. Hiscock and L. Lindblom, “Stability and causality in dissipative relativistic fluids,” *Annals Phys.* **151**, 466–496 (1983).
 - [19] William A. Hiscock and Lee Lindblom, “Generic instabilities in first-order dissipative relativistic fluid theories,” *Phys. Rev. D* **31**, 725–733 (1985).
 - [20] Azwinndini Muronga, “Second order dissipative fluid dynamics for ultrarelativistic nuclear collisions,” *Phys. Rev. Lett.* **88**, 062302 (2002), [Erratum: *Phys.Rev.Lett.* **89**, 159901 (2002)], [arXiv:nucl-th/0104064](#).
 - [21] I. Mäeßler, “Zum paradoxon der wärmeleitungstheorie,” *Zeitschrift für Physik* **198**, 329–344 (1967).
 - [22] W. Israel, “Nonstationary irreversible thermodynamics: A Causal relativistic theory,” *Annals Phys.* **100**, 310–331 (1976).
 - [23] W. Israel and J.M. Stewart, “Transient relativistic thermodynamics and kinetic theory,” *Annals Phys.* **118**, 341–372 (1979).
 - [24] Azwinndini Muronga, “Causal theories of dissipative relativistic fluid dynamics for nuclear collisions,” *Phys. Rev. C* **69**, 034903 (2004), [arXiv:nucl-th/0309055](#).
 - [25] G. S. Denicol, T. Koide, and D. H. Rischke, “Dissipative relativistic fluid dynamics: a new way to derive the equations of motion from kinetic theory,” *Phys. Rev. Lett.* **105**, 162501 (2010), [arXiv:1004.5013 \[nucl-th\]](#).
 - [26] G. S. Denicol, H. Niemi, E. Molnar, and D. H. Rischke, “Derivation of transient relativistic fluid dynamics from the Boltzmann equation,” *Phys. Rev. D* **85**, 114047 (2012), [Erratum: *Phys.Rev.D* **91**, 039902 (2015)], [arXiv:1202.4551 \[nucl-th\]](#).
 - [27] Rudolf Baier, Paul Romatschke, Dam Thanh Son, Andrei O. Starinets, and Mikhail A. Stephanov, “Relativistic viscous hydrodynamics, conformal invariance, and holography,” *JHEP* **04**, 100 (2008), [arXiv:0712.2451 \[hep-th\]](#).
 - [28] Amaresh Jaiswal, Rajeev S. Bhalerao, and Subrata Pal, “New relativistic dissipative fluid dynamics from kinetic theory,” *Phys. Lett. B* **720**, 347–351 (2013), [arXiv:1204.3779 \[nucl-th\]](#).
 - [29] Amaresh Jaiswal, Rajeev S. Bhalerao, and Subrata Pal, “Complete relativistic second-order dissipative hydrodynamics from the entropy principle,” *Phys. Rev. C* **87**, 021901 (2013), [arXiv:1302.0666 \[nucl-th\]](#).
 - [30] A. El, Z. Xu, and C. Greiner, “Third-order relativistic dissipative hydrodynamics,” *Phys. Rev. C* **81**, 041901 (2010), [arXiv:0907.4500 \[hep-ph\]](#).
 - [31] Mohammed Younus and Azwinndini Muronga, “Third order viscous hydrodynamics from the entropy four current,” *Phys. Rev. C* **102**, 034902 (2020), [arXiv:1910.11735 \[nucl-th\]](#).
 - [32] Caio V. P. de Brito and Gabriel S. Denicol, “Third-order relativistic dissipative fluid dynamics from the method of moments,” *Phys. Rev. D* **108**, 096020 (2023), [arXiv:2302.09097](#)

- [nucl-th].
- [33] Pushpa Panday, Amaresh Jaiswal, and Binoy Krishna Patra, “Causal third-order viscous hydrodynamics within relaxation-time approximation,” *Phys. Rev. D* **109**, 096039 (2024), [arXiv:2404.06381 \[hep-ph\]](#).
- [34] P. Van and T. S. Biro, “First order and stable relativistic dissipative hydrodynamics,” *Phys. Lett. B* **709**, 106–110 (2012), [arXiv:1109.0985 \[nucl-th\]](#).
- [35] Fábio S. Bemfica, Marcelo M. Disconzi, and Jorge Noronha, “Causality and existence of solutions of relativistic viscous fluid dynamics with gravity,” *Phys. Rev. D* **98**, 104064 (2018), [arXiv:1708.06255 \[gr-qc\]](#).
- [36] Pavel Kovtun, “First-order relativistic hydrodynamics is stable,” *JHEP* **10**, 034 (2019), [arXiv:1907.08191 \[hep-th\]](#).
- [37] Rajesh Biswas, Sukanya Mitra, and Victor Roy, “Is first-order relativistic hydrodynamics in a general frame stable and causal for arbitrary interactions?” *Phys. Rev. D* **106**, L011501 (2022), [arXiv:2202.08685 \[nucl-th\]](#).
- [38] S. Z. Belenkij and L. D. Landau, “Hydrodynamic theory of multiple production of particles,” *Usp. Fiz. Nauk* **56**, 309 (1955).
- [39] L. D. Landau, “On the multiparticle production in high-energy collisions,” *Izv. Akad. Nauk Ser. Fiz.* **17**, 51–64 (1953).
- [40] J. D. Bjorken, “Highly Relativistic Nucleus-Nucleus Collisions: The Central Rapidity Region,” *Phys. Rev. D* **27**, 140–151 (1983).
- [41] Steven S. Gubser, “Symmetry constraints on generalizations of Bjorken flow,” *Phys. Rev. D* **82**, 085027 (2010), [arXiv:1006.0006 \[hep-th\]](#).
- [42] Steven S. Gubser and Amos Yarom, “Conformal hydrodynamics in Minkowski and de Sitter spacetimes,” *Nucl. Phys. B* **846**, 469–511 (2011), [arXiv:1012.1314 \[hep-th\]](#).
- [43] Hugo Marrochio, Jorge Noronha, Gabriel S. Denicol, Matthew Luzum, Sangyong Jeon, and Charles Gale, “Solutions of Conformal Israel-Stewart Relativistic Viscous Fluid Dynamics,” *Phys. Rev. C* **91**, 014903 (2015), [arXiv:1307.6130 \[nucl-th\]](#).
- [44] Gabriel S. Denicol, Ulrich W. Heinz, Mauricio Martinez, Jorge Noronha, and Michael Strickland, “Studying the validity of relativistic hydrodynamics with a new exact solution of the Boltzmann equation,” *Phys. Rev. D* **90**, 125026 (2014), [arXiv:1408.7048 \[hep-ph\]](#).
- [45] Gabriel S. Denicol, Ulrich W. Heinz, Mauricio Martinez, Jorge Noronha, and Michael Strickland, “New Exact Solution of the Relativistic Boltzmann Equation and its Hydrodynamic Limit,” *Phys. Rev. Lett.* **113**, 202301 (2014), [arXiv:1408.5646 \[hep-ph\]](#).
- [46] Mohammad Nopoush, Radoslaw Ryblewski, and Michael Strickland, “Anisotropic hydrodynamics for conformal Gubser flow,” *Phys. Rev. D* **91**, 045007 (2015), [arXiv:1410.6790 \[nucl-th\]](#).
- [47] M. Martinez, M. McNelis, and U. Heinz, “Anisotropic fluid dynamics for Gubser flow,” *Phys. Rev. C* **95**, 054907 (2017), [arXiv:1703.10955 \[nucl-th\]](#).
- [48] Chandrodoy Chattopadhyay, Ulrich Heinz, Subrata Pal, and Gojko Vujanovic, “Higher order and anisotropic hydrodynamics for Bjorken and Gubser flows,” *Phys. Rev. C* **97**, 064909 (2018), [arXiv:1801.07755 \[nucl-th\]](#).
- [49] Dong-Lin Wang, Xin-Qing Xie, Shuo Fang, and Shi Pu, “Analytic solutions of relativistic dissipative spin hydrodynamics with radial expansion in Gubser flow,” *Phys. Rev. D* **105**, 114050 (2022), [arXiv:2112.15535 \[hep-ph\]](#).
- [50] Yoshitaka Hatta and Bo-Wen Xiao, “Building up the elliptic flow: analytical insights,” *Phys. Lett. B* **736**, 180–185 (2014), [arXiv:1405.1984 \[nucl-th\]](#).
- [51] Umut Gursoy, Dmitri Kharzeev, and Krishna Rajagopal, “Magnetohydrodynamics, charged currents and directed flow in heavy ion collisions,” *Phys. Rev. C* **89**, 054905 (2014), [arXiv:1401.3805 \[hep-ph\]](#).
- [52] Yoshitaka Hatta, Jorge Noronha, Giorgio Torrieri, and Bo-Wen Xiao, “Flow harmonics within an analytically solvable viscous hydrodynamic model,” *Phys. Rev. D* **90**, 074026 (2014), [arXiv:1407.5952 \[hep-ph\]](#).
- [53] Yoshitaka Hatta, Akihiko Monnai, and Bo-Wen Xiao, “Flow harmonics v_n at finite density,” *Phys. Rev. D* **92**, 114010 (2015), [arXiv:1505.04226 \[hep-ph\]](#).
- [54] Partha Bagchi, Arpan Das, and Ananta P. Mishra, “Does Quarkonia Suppression serve as a probe for the deconfinement in small systems?” *Phys. Rev. D* **110**, 014017 (2024), [arXiv:2310.12267 \[nucl-th\]](#).
- [55] Jean-François Paquet, “Thermal photon production in Gubser inviscid relativistic fluid dynamics,” *Phys. Rev. C* **108**, 064912 (2023), [arXiv:2305.10669 \[nucl-th\]](#).
- [56] Ralf Rapp, “Theory of Soft Electromagnetic Emission in Heavy-Ion Collisions,” *Acta Phys. Polon. B* **42**, 2823–2852 (2011), [arXiv:1110.4345 \[nucl-th\]](#).
- [57] Gojko Vujanovic, Jean-François Paquet, Gabriel S. Denicol, Matthew Luzum, Sangyong Jeon, and Charles Gale, “Electromagnetic radiation as a probe of the initial state and of viscous dynamics in relativistic nuclear collisions,” *Phys. Rev. C* **94**, 014904 (2016), [arXiv:1602.01455 \[nucl-th\]](#).
- [58] Gabor David, “Direct real photons in relativistic heavy ion collisions,” *Rept. Prog. Phys.* **83**, 046301 (2020), [arXiv:1907.08893 \[nucl-ex\]](#).
- [59] Piotr Salabura and Joachim Stroth, “Dilepton radiation from strongly interacting systems,” *Prog. Part. Nucl. Phys.* **120**, 103869 (2021), [arXiv:2005.14589 \[nucl-ex\]](#).
- [60] Charles Gale, Jean-François Paquet, Björn Schenke, and Chun Shen, “Multimessenger heavy-ion collision physics,” *Phys. Rev. C* **105**, 014909 (2022), [arXiv:2106.11216 \[nucl-th\]](#).
- [61] Frank Geurts and Ralf-Arno Tripolt, “Electromagnetic probes: Theory and experiment,” *Prog. Part. Nucl. Phys.* **128**, 104004 (2023), [arXiv:2210.01622 \[hep-ph\]](#).
- [62] Maurice Coquet, Xiaojian Du, Jean-Yves Ollitrault, Soeren Schlichting, and Michael Winn, “Transverse mass scaling of dilepton radiation off a quark-gluon plasma,” *Nucl. Phys. A* **1030**, 122579 (2023), [arXiv:2112.13876 \[nucl-th\]](#).
- [63] Maurice Coquet, Michael Winn, Xiaojian Du, Jean-Yves Ollitrault, and Soeren Schlichting, “Dilepton Polarization as a Signature of Plasma Anisotropy,” *Phys. Rev. Lett.* **132**, 232301 (2024), [arXiv:2309.00555 \[nucl-th\]](#).
- [64] R. Baier, B. Pire, and D. Schiff, “Dilepton production at finite temperature: Perturbative treatment at order α_s ,” *Phys. Rev. D* **38**, 2814 (1988).
- [65] K. Haglin, Charles Gale, and V. Emel’yanov, “Soft dilepton production in relativistic heavy ion collisions,” *Phys. Rev. D* **47**, 973–988 (1993), [arXiv:hep-ph/9208211](#).
- [66] P. Aurenche, F. Gelis, R. Kobes, and H. Zaraket, “Bremsstrahlung and photon production in thermal QCD,” *Phys. Rev. D* **58**, 085003 (1998), [arXiv:hep-ph/9804224](#).
- [67] Peter Brockway Arnold, Guy D. Moore, and Laurence G. Yaffe, “Photon emission from quark gluon plasma: Complete leading order results,” *JHEP* **12**, 009 (2001), [arXiv:hep-ph/0111107](#).
- [68] Peter Brockway Arnold, Guy D. Moore, and Laurence G. Yaffe, “Photon emission from ultrarelativistic plasmas,” *JHEP* **11**, 057 (2001), [arXiv:hep-ph/0109064](#).
- [69] Peter Brockway Arnold, Guy D. Moore, and Laurence G. Yaffe, “Effective kinetic theory for high temperature gauge the-

- ories,” *JHEP* **01**, 030 (2003), [arXiv:hep-ph/0209353](#).
- [70] Jacopo Ghiglieri and Guy D. Moore, “Low Mass Thermal Dilepton Production at NLO in a Weakly Coupled Quark-Gluon Plasma,” *JHEP* **12**, 029 (2014), [arXiv:1410.4203 \[hep-ph\]](#).
- [71] Matthew Heffernan, Paul Hohler, and Ralf Rapp, “Universal Parametrization of Thermal Photon Rates in Hadronic Matter,” *Phys. Rev. C* **91**, 027902 (2015), [arXiv:1411.7012 \[hep-ph\]](#).
- [72] Niklas Götz, Anna Schäfer, Oscar Garcia-Montero, Jean-François Paquet, Hannah Elfner, and Charles Gale (SMASH), “Out-of-equilibrium photon production in the late stages of relativistic heavy-ion collisions,” *Phys. Rev. C* **105**, 044910 (2022), [Erratum: *Phys.Rev.C* 109, 049901 (2024)], [arXiv:2111.13603 \[hep-ph\]](#).
- [73] Jessica Churchill, Lipai Du, Charles Gale, Greg Jackson, and Sangyong Jeon, “Dilepton production at next-to-leading order and intermediate invariant-mass observables,” *Phys. Rev. C* **109**, 044915 (2024), [arXiv:2311.06675 \[nucl-th\]](#).
- [74] L. Oliva, M. Ruggieri, S. Plumari, F. Scardina, G. X. Peng, and V. Greco, “Photons from the Early Stages of Relativistic Heavy Ion Collisions,” *Phys. Rev. C* **96**, 014914 (2017), [arXiv:1703.00116 \[nucl-th\]](#).
- [75] Maurice Coquet, Xiaojian Du, Jean-Yves Ollitrault, Soeren Schlichting, and Michael Winn, “Intermediate mass dileptons as pre-equilibrium probes in heavy ion collisions,” *Phys. Lett. B* **821**, 136626 (2021), [arXiv:2104.07622 \[nucl-th\]](#).
- [76] Jessica Churchill, Li Yan, Sangyong Jeon, and Charles Gale, “Emission of electromagnetic radiation from the early stages of relativistic heavy-ion collisions,” *Phys. Rev. C* **103**, 024904 (2021), [arXiv:2008.02902 \[hep-ph\]](#).
- [77] Xiang-Yu Wu, Han Gao, Bailey Forster, Charles Gale, Greg Jackson, and Sangyong Jeon, “Thermal dilepton polarization and dynamics of the QCD plasma in relativistic heavy-ion collisions,” (2024), [arXiv:2412.15052 \[nucl-th\]](#).
- [78] Oscar Garcia-Montero, Aleksas Mazeliauskas, Philip Plaschke, and Sören Schlichting, “Pre-equilibrium photons from the early stages of heavy-ion collisions,” *JHEP* **03**, 053 (2024), [arXiv:2308.09747 \[hep-ph\]](#).
- [79] Oscar Garcia-Montero, Philip Plaschke, and Sören Schlichting, “Scaling of pre-equilibrium dilepton production in QCD kinetic theory,” *Phys. Rev. D* **111**, 034036 (2025), [arXiv:2403.04846 \[hep-ph\]](#).
- [80] Ralf Rapp and Hendrik van Hees, “Thermal Dileptons as Fireball Thermometer and Chronometer,” *Phys. Lett. B* **753**, 586–590 (2016), [arXiv:1411.4612 \[hep-ph\]](#).
- [81] S. D. Drell and Tung-Mow Yan, “Massive Lepton Pair Production in Hadron-Hadron Collisions at High-Energies,” *Phys. Rev. Lett.* **25**, 316–320 (1970), [Erratum: *Phys.Rev.Lett.* 25, 902 (1970)].
- [82] Kevin Dusling and Shu Lin, “Dilepton production from a viscous QGP,” *Nucl. Phys. A* **809**, 246–258 (2008), [arXiv:0803.1262 \[nucl-th\]](#).
- [83] Jitesh R. Bhatt and V. Sreekanth, “Photon emission from out of equilibrium dissipative parton plasma,” *Int. J. Mod. Phys. E* **19**, 299–306 (2010), [arXiv:0901.1363 \[hep-ph\]](#).
- [84] Jitesh R. Bhatt, Hiranmaya Mishra, and V. Sreekanth, “Thermal photons in QGP and non-ideal effects,” *JHEP* **11**, 106 (2010), [arXiv:1011.1969 \[hep-ph\]](#).
- [85] Jitesh R. Bhatt, Hiranmaya Mishra, and V. Sreekanth, “Cavitation and thermal dilepton production in QGP,” *Nucl. Phys. A* **875**, 181–196 (2012), [arXiv:1101.5597 \[hep-ph\]](#).
- [86] Rajeev S. Bhalerao, Amaresh Jaiswal, Subrata Pal, and V. Sreekanth, “Particle production in relativistic heavy-ion collisions: A consistent hydrodynamic approach,” *Phys. Rev. C* **88**, 044911 (2013), [arXiv:1305.4146 \[nucl-th\]](#).
- [87] Gojko Vujanovic, Clint Young, Bjoern Schenke, Ralf Rapp, Sangyong Jeon, and Charles Gale, “Dilepton emission in high-energy heavy-ion collisions with viscous hydrodynamics,” *Phys. Rev. C* **89**, 034904 (2014), [arXiv:1312.0676 \[nucl-th\]](#).
- [88] Vinod Chandra and V. Sreekanth, “Quark and gluon distribution functions in a viscous quark-gluon plasma medium and dilepton production via $q\bar{q}$ annihilation,” *Phys. Rev. D* **92**, 094027 (2015), [arXiv:1511.01208 \[nucl-th\]](#).
- [89] Lakshmi J. Naik and V. Sreekanth, “Second order hydrodynamics based on effective kinetic theory and electromagnetic signals from QGP,” *J. Phys. G* **50**, 025102 (2023), [arXiv:2207.05310 \[nucl-th\]](#).
- [90] Rajeev S. Bhalerao, Amaresh Jaiswal, Subrata Pal, and V. Sreekanth, “Relativistic viscous hydrodynamics for heavy-ion collisions: A comparison between the Chapman-Enskog and Grad methods,” *Phys. Rev. C* **89**, 054903 (2014), [arXiv:1312.1864 \[nucl-th\]](#).
- [91] Aleks Kurkela and Yan Zhu, “Isotropization and hydrodynamization in weakly coupled heavy-ion collisions,” *Phys. Rev. Lett.* **115**, 182301 (2015), [arXiv:1506.06647 \[hep-ph\]](#).
- [92] Michal P. Heller, Aleks Kurkela, Michal Spaliński, and Viktor Svensson, “Hydrodynamization in kinetic theory: Transient modes and the gradient expansion,” *Phys. Rev. D* **97**, 091503 (2018), [arXiv:1609.04803 \[nucl-th\]](#).
- [93] Gabriel Denicol and Dirk Rischke, “Microscopic foundations of relativistic fluid dynamics,” *Lecture Notes in Physics* (2021), 10.1007/978-3-030-82077-0.
- [94] Ramona Vogt, *Ultrarelativistic heavy-ion collisions* (Elsevier, Amsterdam, 2007).
- [95] Taesoo Song, Kyong Chol Han, and Che Ming Ko, “Dilepton production in a schematic causal viscous hydrodynamics,” *Phys. Rev. C* **83**, 024904 (2011), [arXiv:1012.0798 \[nucl-th\]](#).
- [96] Lakshmi J. Naik, Sunil Jaiswal, K. Sreelakshmi, Amaresh Jaiswal, and V. Sreekanth, “Hydrodynamical attractor and thermal particle production in heavy-ion collision,” (2021), [arXiv:2107.08791 \[hep-ph\]](#).
- [97] Lakshmi J. Naik, Sunil Jaiswal, K. Sreelakshmi, Amaresh Jaiswal, and V. Sreekanth, “Analytical attractors and thermal particle spectra from quark-gluon plasma,” *DAE Symp. Nucl. Phys.* **65**, 660–661 (2021).
- [98] K. Dusling and D. Teaney, “Simulating elliptic flow with viscous hydrodynamics,” *Phys. Rev. C* **77**, 034905 (2008), [arXiv:0710.5932 \[nucl-th\]](#).
- [99] Radoslaw Ryblewski and Michael Strickland, “Dilepton production from the quark-gluon plasma using (3+1)-dimensional anisotropic dissipative hydrodynamics,” *Phys. Rev. D* **92**, 025026 (2015), [arXiv:1501.03418 \[nucl-th\]](#).